Microchimica Acta (2021) 188: 392
https://doi.org/10.1007/s00604-021-05033-3

ORIGINAL PAPER

Point-of-care testing of butyrylcholinesterase activity through modulating the photothermal effect of cuprous oxide nanoparticles

Jinzhu Ma[1] · Lili Ma[1] · Lili Cao[1] · Yuming Miao[1] · Jiangxue Dong[1] · Yu-e Shi[1] · Zhenguang Wang[1]

Received: 17 August 2021 / Accepted: 15 September 2021 / Published online: 25 October 2021

Abstract

Butyrylcholinesterase (BChE) is an important indicator for clinical diagnosis of liver dysfunction, organophosphate toxicity, and poststroke dementia. Point-of-care testing (POCT) of BChE activity is still a challenge, which is a critical requirement for the modern clinical diagnose. A portable photothermal BChE assay is proposed through modulating the photothermal effects of Cu_2O nanoparticles. BChE can catalyze the decomposition of butyrylcholine, producing thiocholine, which further reduce and coordinate with CuO on surface of Cu_2O nanoparticle. This leads to higher efficiency of formation of Cu_9S_8 nanoparticles, through the reaction between Cu_2O nanoparticle and NaHS, together with the promotion of photothermal conversion efficiency from 3.1 to 59.0%, under the excitation of 1064 nm laser radiation. An excellent linear relationship between the temperature change and the logarithm of BChE concentration is obtained in the range 1.0 to 7.5 U/mL, with a limit of detection of 0.076 U/mL. In addition, the portable photothermal assay shows strong detection robustness, which endows the accurate detection of BChE in human serum, together with the screening and quantification of organophosphorus pesticides. Such a simple, sensitive, and robust assay shows great potential for the applications to clinical BChE detection and brings a new horizon for the development of temperature based POCT.

Keywords Butyrylcholinesterase · Point-of-care testing · Fluorescence detection · Photothermal effect · Cuprous oxide · CuO nanoparticles

Introduction

Butyrylcholinesterase (BChE) is a type of nonspecific cholinesterase enzyme that can hydrolyze choline-based esters, which is produced in the liver and then quickly released to the blood [1, 2]. The normal concentration of BChE in human serum is in the range from 6900 to 11,000 U/L, and its low expression level is related with many diseases, such as liver dysfunction, Alzheimer's disease, organophosphate toxicity, and poststroke dementia [2, 3]. In addition, a low level of BChE would lead to the delayed metabolism of several important clinical compounds, such as cocaine, procaine, and succinylcholine [2]. Thus, the sensitive and fast detection of BChE activity is highly desired. To date, many strategies have been developed for the sensitive and selective detection of BChE activity, by using the facilities of absorbance spectrometer [4], fluorescence spectrometer [5], Raman spectrometer [6], mass spectrometer [7], and electrochemical workstation [8]. However, it is still difficult to realize point-of-care testing (POCT) of BChE activity, which is a critical requirement for the modern clinical diagnose.

Thermometer is one of the most frequently used devices in daily life, which is portable, easy to operate, and low cost. Photothermal effect is a common phenomenon that the photoexcitation of materials leads to the increase of thermal energy and temperature [9–11]. Photothermal effect shows great advantages for developing POCT assays, due to its features of miniaturization, nondestructive testing, and ease of operation. The challenge in developing photothermal assay is to link the process of target binding with a temperature

✉ Yu-e Shi
shiyue1220@163.com

✉ Zhenguang Wang
zwang65-c@my.cityu.edu.hk

[1] Key Laboratory of Chemical Biology of Hebei Province, Key Laboratory of Medicinal Chemistry and Molecular Diagnosis, Ministry of Education, College of Chemistry & Environmental Science, Hebei University, Baoding 071002, China

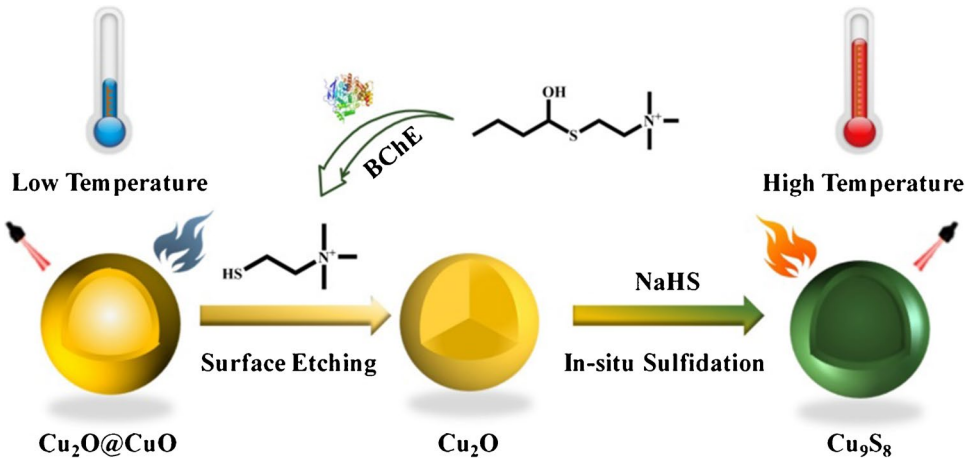

Scheme 1 Schematic illustration for the photothermal detection of BChE through modulating the photothermal effects of Cu_2O nanoparticles

output [12, 13]. Fu et al. proposed the first photothermal assay for prostate-specific antigen, based on the classical enzyme-linked immunosorbent assay using iron oxide nanoparticles mediated Prussian blue (PB) as photothermal probes [14]. Several groups also engaged in developing photothermal assay for BChE. For example, Wang's group reported a portable photothermal device for BChE detection, where BChE can trigger the photothermal signal by in situ producing PB through the reaction between MIL-53 (Fe) and the hydrolysis product of BChE and substrate [15]. We have also developed a photothermal assay for BChE activity by modulating the process of MnO_2 nanosheet-assisted dopamine polymerization [16]. However, they are still suffering from the problems of relatively low photothermal conversion efficiency, complicacy in synthesis, and separation process. Therefore, developing innovative photothermal materials and straightforward photothermal sensing strategies for POCT of BChE activity is still highly desirable.

Cuprous oxide (Cu_2O) nanostructures show great potential for developing chemical assays, featuring low toxicity, narrow and tunable bandgap, and p-type characters [17, 18]. The morphology and size of Cu_2O can be well controlled through wet-chemical synthesis strategies [19]. They also show excellent coordination ability with various chemical groups, such as -COOH, $-NH_2$, -SH [20, 21]. However, the applications of Cu_2O nanostructures as photothermal materials have been rarely reported, limited by their relatively low absorption ability in the NIR region. In this work, a photothermal assay for BChE activity is developed through modulating the photothermal effect of Cu_2O nanoparticles (Scheme 1). The surface of Cu_2O nanoparticles can be etched by thiocholine, decomposition product of butyrylcholine under the catalyzing of BChE, which further produces Cu_9S_8 nanoparticles through reaction with NaHS. The photothermal conversion efficiency is promoted from 3.1 to 59.0%. Thus, the activity of BChE can be quantitatively converted into the photothermal effect of system, and a linear relationship between the temperature change and the logarithm of BChE concentration is obtained in the range from 1.0 to 7.5 U/mL. The assay also shows excellent detection performances for BChE in human serum, and it is also used to screen and detect organophosphorus pesticides.

Experimental section

Materials

Copper acetate monohydrate, ethylene glycol, polyvinylpyrrolidone (PVP), and L-glutamine (Gln) were obtained from Aladdin. Sodium hydrosulfide (NaHS), glucose (Glu), zinc nitrate hexahydrate ($Zn(NO_3)_2$), L(+)-ascorbic acid (Vc), cysteamine (Cys), potassium chloride (KCl), sodium chloride (NaCl), calcium chloride dehydrate ($CaCl_2 \bullet 2H_2O$), L-histidine (His), L-alanine (Ala), and L(+)-glutamic acid (Gla) were obtained from Innochem. Butyrylcholinesterase (BChE, 14 units/mg protein, from Equine serum), acetylthiocholine (ATCh) iodide (≥98%), acetylcholinesterase (AChE, 200–1,000 units/mg protein, from electrophorus electricus), and butyrylcholine (BTCh) chloride (≥98%) were obtained from Sigma-Aldrich.

Instrumentation

The morphologies of the Cu_2O and Cu_9S_8 nanoparticles were characterized by using a scanning electron microscope (SEM; JSM-7500, Japan) and a transmission electron microscopy (TEM; FEI Tecnai G2 F20 S-TWIN, USA). A photoelectron spectrometer (XPS; ESCALAB-MK II 250, Thermo, USA) was used to record the XPS spectra of samples. Powder X-ray diffraction (XRD) patterns were recorded on an X-ray diffractometer (D8 ADVANCE, Bruker, USA). The Raman spectra were recorded on a high-resolution Horiba Jobin–Yvon LabRAM-800 Raman spectrophotometer.

The absorption spectra were recorded by using an absorption spectrophotometer (UV3600; Shimadzu, Japan).

Synthesis of the Cu_2O Nanoparticles and their in situ *sulfidation*

Cu_2O nanoparticles were synthesized according to the previous works [19]. For in situ sulfidation reaction, 10 μL of Cu_2O nanoparticles (2.2 mM) was mixed with 40 μL of NaHS solution (20 mM), which was allowed to react for 2 h under room temperature, until the color of mixture changed into dark green.

Detection of BChE activity

Different concentrations of BChE (10 μL) were mixed with 6 mM BTCh (10 μL), which is allowed to react for 40 min. Then, 10 μL of Cu_2O nanoparticles (2.2 mM) and 40 μL of NaHS solution (20 mM) were injected into above mixture and incubated for 1 h. The temperature of system was recoded an infrared thermal imager after irradiated by a 1064 nm laser for 10 min.

To evaluate the selectivity of our assay for BChE detection, we challenged it to various interference species. BChE was replaced by different chemicals including Na^+, K^+, Mg^{2+}, Ca^{2+}, Zn^{2+}, Fe^{3+}, Glu, Ala, His, Gla, Gln, Vc, and Cys, and the sequent detection progresses were same with that of BChE detection. The selectivity of our assay to AChE was conducted by recording the temperature changes of different enzymes AChE and BChE (6 U/mL) and their combinations with different substrates ATCh and BTCh (6 mM) under the same process and conditions as that BChE detection.

Calculation of the photothermal conversion efficiency

The photothermal conversion efficiency (η) of Cu_2O, Cu_9S_8, and Cu_9S_8-BChE can be calculated according to Eq. 1:

$$\eta = \frac{mc(T_{max} - T_{max,H_2O})}{I(1 - 10^{-A})\tau_s} \quad (1)$$

where T_{max} is the maximum of temperature under the irradiation of laser; m is the mass of the solution; C is equal to 4.2 J/g; and A is the absorbance of the solution of nanomaterials at 1064 nm. τ_s is a constant number for a given materials, and it is calculated according to Eq. 2:

$$t = -\tau_s \bullet \ln\left(\frac{T - T_{surr}}{T_{max} - T_{surr}}\right) = -\tau_s \bullet \ln(\theta) \quad (2)$$

where T_{surr} is the temperature of environment and t is the time responding to the real-time temperature change. The τ_s for Cu_2O, Cu_9S_8, and Cu_9S_8-BChE can be calculated to be 251, 138, and 120 s, respectively. Thus, the η of Cu_2O, Cu_9S_8, and Cu_9S_8-BChE is calculated to be 3.1%, 35.8%, and 59.0%, respectively. The number of these characters is listed in the Table S1.

Results and discussion

Characterization of the Cu_2O nanoparticles and their in situ *sulfidation*

Cu_2O nanoparticles were selected as the photothermal materials, due to their features of low toxicity, narrow and tunable bandgap, and easy of coordination with thiols. In addition, Cu_2O nanoparticles can be conveniently converted to other forms, under external stimulations [19]. Cu_2O nanoparticles were synthesized through the reduction of Cu^{2+} by AA

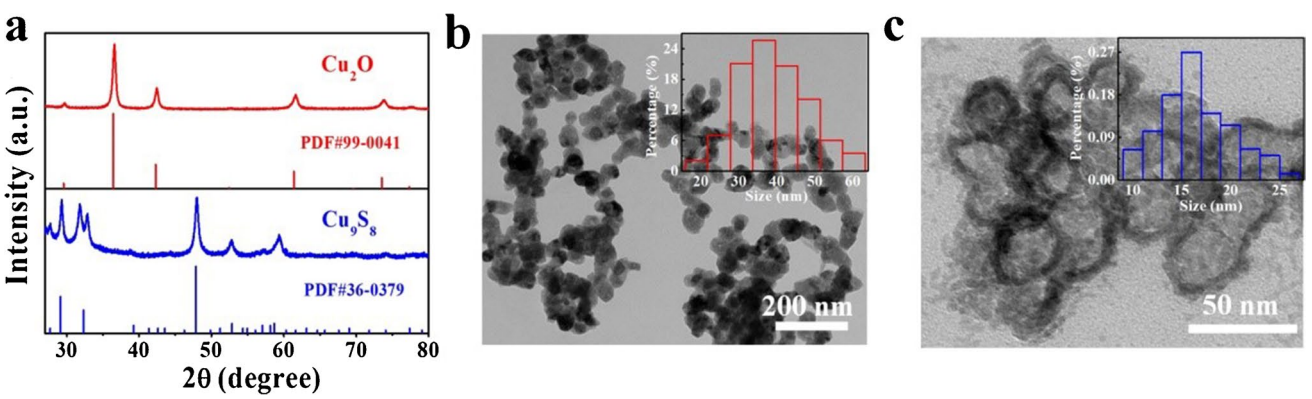

Fig. 1 Characterization of Cu_2O nanoparticles and their in situ sulfidation. XRD patterns (**a**), TEM images (**b**, **c**) of Cu_2O, Cu_9S_8 nanoparticles

under the stabilization of PVP, which were further allowed to in situ react with NaHS. The XRD patterns confirm the formation of Cu_2O nanoparticles (Fig. 1a). Obvious peaks located at 36.4, 42.4, 61.6, and 73.8 degree can be observed, corresponding to the (111), (200), (220), and (311) planes of Cu_2O, respectively [22]. After in situ sulfidation, the characterized peaks of Cu_2O disappear, and the strongest peak moves to 48.0 degree, with several satellite peaks at 59.3, 52.8, 31.8, and 29.3 degree, which well matched with Cu_9S_8 (Fig. 1a) [23]. The TEM images shows that the as-prepared Cu_2O nanoparticles are quasi-spherical in shape with an average diameter of 35 nm, which transfers into hollow Cu_9S_8 nanoparticles with a size of 27 nm (Fig. 1 b and c). SEM images suggest the well dispersion and uniform size distribution of both Cu_2O and Cu_9S_8 nanoparticles (Figure S1). The full XPS scan spectra suggest the Cu_2O nanoparticles containing mainly C, O, and Cu. After in situ reaction with NaHS, obvious signal of S can be recognized (Figure S2). High-resolution XPS Cu spectrum of Cu_2O nanoparticles displays two obvious peaks at 951.9 and 932.1 eV, assigned to the Cu $_{2p1/2}$ and Cu $_{2p3/2}$ of Cu^+, respectively (Fig. 2a) [17]. Several satellite peaks are also recorded, including 962.5, 954.1, 944.0, and 942.1 eV, which is the typical features Cu^{2+} of CuO [24]. These results suggest that partial of the Cu_2O nanoparticles were oxidized into CuO during the washing, drying, or storing processes. After reaction with NaHS, the satellite peaks corresponding to Cu^{2+} of CuO disappear, and the peaks located at 951.9 and 932.1 eV become the dominant signal. This suggests that CuO is etched during the formation of Cu_9S_8 nanoparticles [24]. The FTIR spectra also suggest the obvious change on the structures after in situ sulfidation of Cu_2O nanoparticles, with multiple new peaks emerged in the range from 600 to 1300 cm^{-1} (Fig. 2b).

Modulation on photothermal effect of Cu_2O nanoparticles

A prerequisite for designing photothermal assay is the target response light absorption ability, especially in the near infrared (NIR) range [25]. Cu_2O nanoparticle presents a rather weak and nearly negligible absorption in the wavelength from 700 to 1200 nm. Interestingly, introducing of NaHS results in the obvious increase on the absorption, and a hook-like spectrum is recorded in the range from 700 to 1200 nm. Unexpectedly, adding BChE and corresponding substrate (BTCh) into the mixture of Cu_2O nanoparticle and NaHS further promotes the absorption intensities (Fig. 2c), which is called Cu_9S_8-BChE. Accompanied with the change of absorption intensities, their photothermal properties also show huge differences. To calculate the photothermal conversion efficiency (η) of Cu_2O, Cu_9S_8, and Cu_9S_8-BChE, their temperature profiles are recorded by irradiating them with 1064 laser for 20 min, followed by turning off the laser and naturally cooling down (Fig. 3a) [26]. After transferring Cu_2O to Cu_9S_8 and Cu_9S_8-BChE, the η has been greatly promoted from 3.1 to 35.8%, and 59.0%, respectively. The details about calculations are presented in the "Experimental section." The efficiency is much higher than the cases of MnO_2 nanosheets [16], $Cu_{2-x}Se$ nanocrystals, and $Cu_3(PO_4)_2$ nanosheets coated with polydopamine, which is even comparable with the gold nanoparticles [4]. The high photothermal efficiency can be attributed to the high absorption ability in the wavelength from 700 to 1200 nm and the reflex effect of the rough surface of Cu_9S_8.

To study the mechanism of promotion on photothermal effect after introducing BChE and substrate, the UV–visible absorption spectra of the reaction system are collected. Intensive absorption bands located at 472, 381, and 295 nm can be observed on Cu_2O nanoparticles (Fig. 3b, Figure S3). The absorption bands located at 472 nm can be attributed to

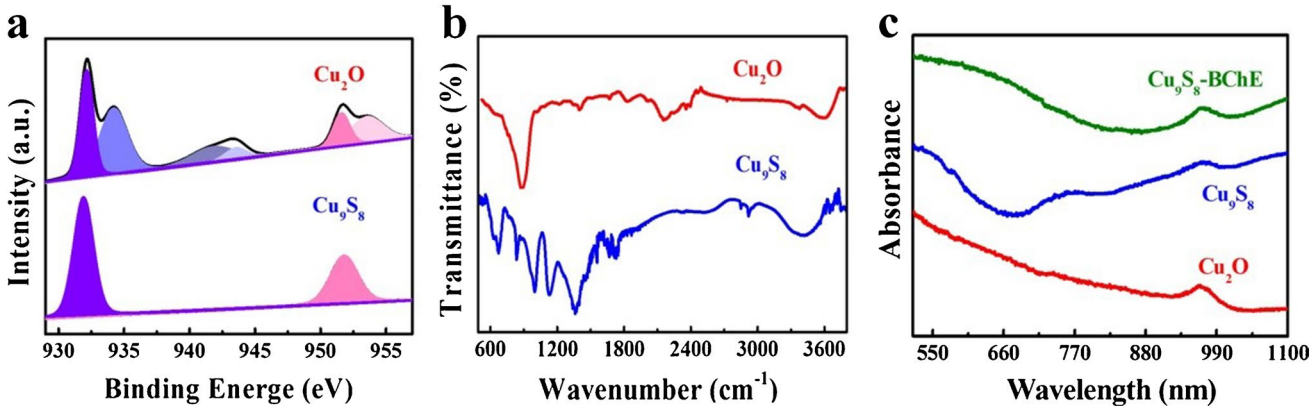

Fig. 2 **a** High-resolution XPS spectrum of Cu $_{2p}$ electrons, **b** FTIR spectra of Cu_2O and Cu_9S_8 nanoparticles; **c** UV–visible absorption spectra of Cu_2O, Cu_9S_8 nanoparticles, and Cu_9S_8 produced in the presence of BChE (6 U/mL)

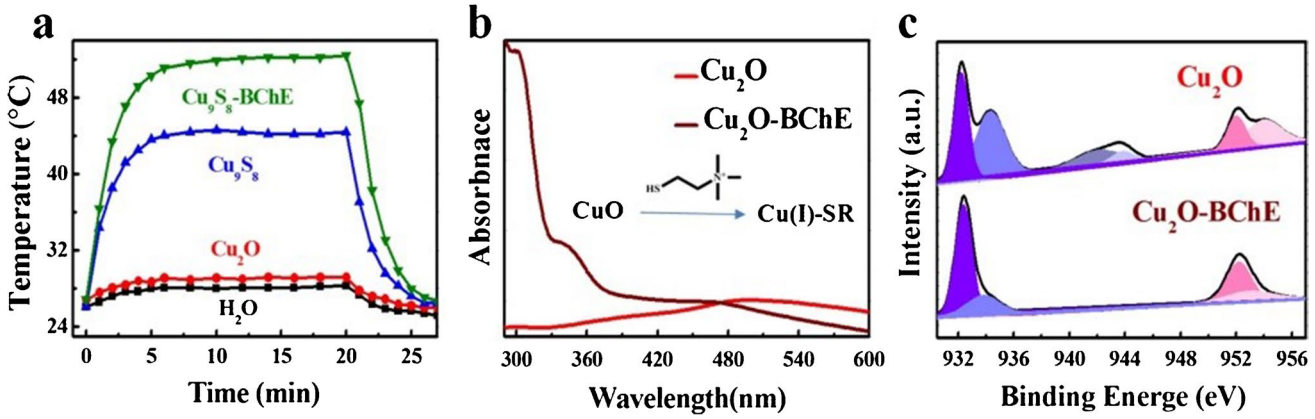

Fig. 3 Temperature profiles of pure water, Cu_2O, Cu_9S_8 nanoparticles, and Cu_9S_8 produced in the presence of BChE (**a**). UV–visible absorption spectra (**b**) and high-resolution XPS spectrum of Cu $_{2p}$ electrons (**c**) of Cu_2O nanoparticles and after reaction with BChE

the optical bandgap of Cu_2O nanoparticles, consistent with previously reported experimentally and theoretical works [27], while the absorption at shorter wavelength can be attributed to the disorder-related sub-bandgap states, caused by the defects originated from the amorous regions or the CuO layers [17]. After mixing with BChE and substrate, above characterized peaks disappear, and two obvious peaks located at 302 and 346 nm become the dominant peaks, attributed to complex of Cu^+ with thiols (Fig. 3b) [28–30]. Thus, introducing of BChE results in the etching of CuO on surface of Cu_2O nanoparticles by forming Cu(I)-SR complex. XPS results also suggest that introducing BChE eliminates the satellite peaks of CuO, located at 962.5, 954.1, 944.0, and 942.1 eV, on the surface of Cu_2O nanoparticles (Fig. 3c) [31]. Only the peaks located at 951.9 and 932.1 eV are reserved, corresponding to Cu^+, which confirms the etching of CuO. Based on above information, we proposed a surface-etched mechanism for explaining the promoted photothermal effect after introducing BChE. BChE can catalyze the decomposition of BTCh, producing thiocholine, which further reduce and coordinate with CuO. This etches the surface production layer of Cu_2O nanoparticle, leading to the higher efficiency on formation of Cu_9S_8, together with promoted photothermal effect.

Detection of BChE activity

The η has an exponential relationship with the absorption properties of materials, which is related with their concentration. Thus, the heat released from the Cu_9S_8-BChE under light irradiation should correlate with the concentration of BChE. We challenged our system with various concentration of BChE, and their temperature profiles were recorded. As expected, the value of temperature change ($\Delta T - \Delta T_0$) increases with the increasing of BChE concentration, where ΔT and ΔT_0 is defined as the value of temperature change in the absence and presence of BChE and the substrate, under the irradiation of 1064 nm laser (Fig. 4a). An excellent linear relationship between $\Delta T - \Delta T_0$ and the logarithm of BChE concentration in the range from 1.0 to 7.5 U/mL can be observed, with a linear regression equation of $\Delta T - \Delta T_0 = 6.62 \log [BChE] + 3.07$, $R^2 = 0.991$. A limit of detection (LOD) of 0.076 U/mL was calculated, based on the rules of 3 times signal-to-noise ratio. The LOD of our assay is better than the portable BChE assays, such as Ellman's colorimetric assay and the commercial ELISA Kit for BChE [32]. In addition, the detection performances of our assay are equal to or better than the previous works that used expensive and complicated instruments (Table S2).

Evaluation on the selectivity of the photothermal assay

To test the practical applications of our assay, the effects of various interfering species, such as metal ions, amino acids, and common small biomolecules, on the value of ΔT were studied. The concentration of above species is adjusted to their normal levels in human serum, as shown in Table S3. As shown in Fig. 4b, BChE can trigger an obvious increase on the temperature, compared with that of blank samples. The value of ΔT is almost same with that of blank samples, when adding Zn^{2+}, Fe^{3+}, Ala, His, and Cys into the system. A fluctuation of less than 20% with that of BChE is observed on the value of ΔT, in the cases of Na^+, K^+, Fe^{3+}, Mg^{2+}, Glu, Gla, and Vc, indicating the high detection robustness of our assay. The interferences of AChE were also assessed, by recording the value of ΔT after adding different combination of AChE, BChE, BTCh, and ATCh. Results in Fig. 4c show that the value of ΔT is almost identical to that of blank samples when AChE

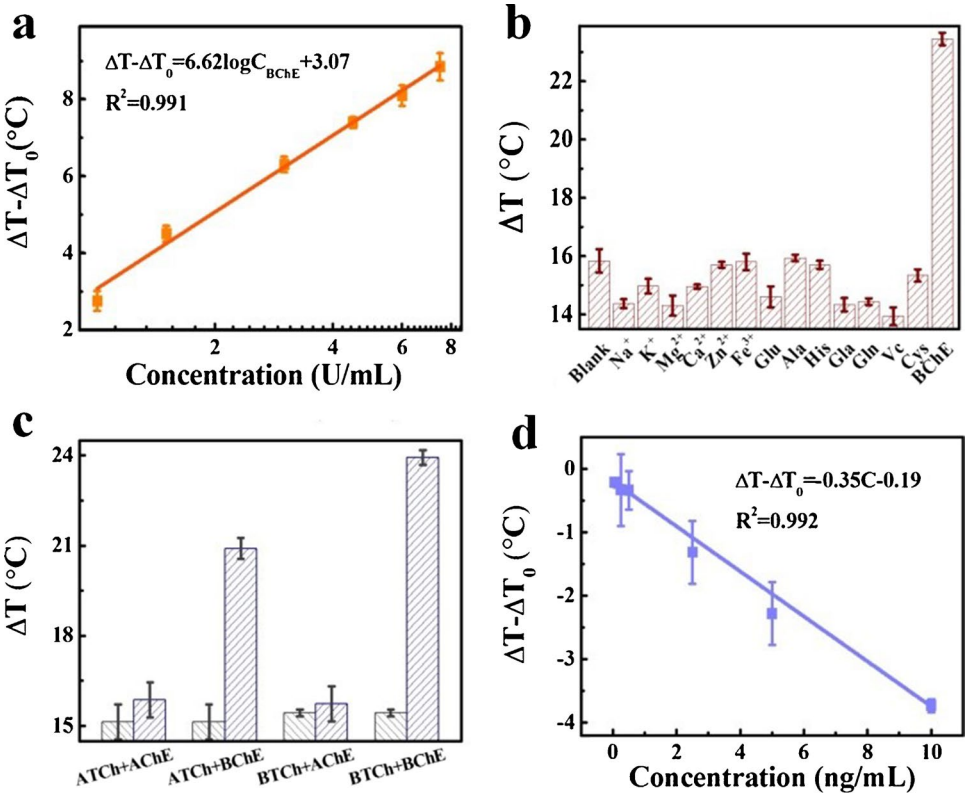

Fig. 4 Relationship between the value of temperature change and the concentration of BChE (**a**). Selectivity evaluation of our assay towards various interfering specifics (**b**) and towards AChE and different combinations with substrates (**c**); blank stands for the temperature change of the system without adding any chemicals excepting the buffer; linear relationship between the value of temperature change and the concentration of paraoxon. All the temperature values were recorded on an IR camera under the excitation of 1064 nm laser

is combined with BTCh. Remarkable increase on ΔT is observed after adding same amount of BChE. Both AChE and BChE can trigger the efficient temperature change, when ATCh is utilized as the substrate. These results suggest that the photothermal assay has a good selectivity towards AChE, once BTCh is used as the substrate.

Quantitative detection of BChE in human serum

In view of the high detection performances of our photothermal assay, it was further challenged to detect the BChE activity in human serum samples. The clinical serum sample of healthy people was directly added into the system, and the concentration of BChE is detected to be 10,034 U/L, based on the calibration curve presented in Figure S4. This result falls into the normal range of healthy people (9010 ± 2041 U/L), which suggests the clinical application potential of our assay. The detection accuracy of photothermal assay is further evaluated through standard addition experiments. Different concentrations (4, 6, and 8 U/mL) of BChE are spilled into human serum sample, which was regarded as regular sample for sequent detection. The concentration of 4, 6, and 8 U/mL are selected for the spiking experiments. The concentration is located in the middle region of our linear range, which is suitable for quantitative study, and we intended to choose the three concentrations with minor difference to evaluate the accuracy of the assay. Obvious changes on the value of $\Delta T - \Delta T_0$ can be observed even with a minor change on the concentration of BChE, and satisfactory recoveries can be obtained, in the range from 99.6 to 101.5%, which suggests the reliability and accuracy of our assay (Table S4). However, the nature of easy of oxidation and reaction with acid of Cu-based nanomaterials should be addressed for applications in some hash environments, such as high concentration acid and oxidants.

BChE inhibition screening

The photothermal assay is further used to study the inhibition of BChE activity of organophosphorus pesticides. Paraoxon, one of the most potent cholinesterase-inhibiting insecticides, is selected as an example. As shown in Fig. 3d, a decreased value of $\Delta T - \Delta T_0$ can be observed with the increasing concentration of paraoxon, and a linear relationship between the value and the concentration is achieved in the range from 0.05 to 10 ng/mL (Fig. 4d). A linear regression equation of $\Delta T = -0.35$ [paraoxon] $- 0.19$, $R^2 = 0.992$ is obtained, and a LOD of $1.73*10^{-3}$ ng/mL is calculated, based on the rules of 3 times signal-to-noise ratio. The LOD of our portable photothermal assay is comparable or better than most of the reported works (Table S5).

Conclusions

A POCT method for BChE is developed based on the coordination reaction between the thiocholine, decomposition product of butyrylcholine catalyzed by BChE, and the CuO layer on surface of Cu_2O nanoparticle. With the aid of NaHS, the Cu_2O nanoparticle was transferred into Cu_9S_8 nanoparticles, and a promotion on the photothermal conversion efficiency from 3.1 to 59.0% was observed. The photothermal assay shows a good sensitivity for BChE and reasonable detection robustness against various interfere species. The assay is further used for direct detection of BChE in human serum and screening and quantification of organophosphorus pesticides. The strategies for detection pathways and modulation of photothermal effects presented here constitute a new door towards POCT of biomolecules, which also widen the scope of applications for Cu_2O nanoparticles. However, the nature of easy of oxidation for Cu-based nanomaterials should be addressed for applications in some hash environments, such as high concentration acid and oxidants.

Supplementary Information The online version contains supplementary material available at https://doi.org/10.1007/s00604-021-05033-3.

Funding This work was financially supported by the National Natural Science Foundation of China (21804030, 22007027), the Natural Science Foundation of Hebei Province (B2019201067), the Outstanding Youth Project of Natural Science Foundation of Hebei Province (B2020201060), One Hundred Talent Project of Hebei Province (E2019050011), and Science and Technology Project of Hebei Education Department (BJ2020033).

Declarations

Conflict of interest The authors declare no competing interests.

References

1. Ellman GL, Courtney KD, Andres V, Featherstone RM (1961) A new and rapid colorimetric determination of acetylcholinesterase activity. Biochem Pharmacol 7(2):88–95
2. Williams A, Zhou S, Zhan C-G (2019) Discovery of potent and selective butyrylcholinesterase inhibitors through the use of pharmacophore-based screening. Bioorg. Med. Chem. Lett. 29(24):126754
3. Lockridge O (2015) Review of human butyrylcholinesterase structure, function, genetic variants, history of use in the clinic, and potential therapeutic uses. Pharmacol Ther 148:34–46
4. Zhang J, Mou L, Jiang X (2018) Hydrogels incorporating Au@polydopamine nanoparticles: robust performance for optical sensing. Anal Chem 90(19):11423–11430
5. Chen G, Feng H, Jiang X, Xu J, Pan S, Qian Z (2018) Redox-controlled fluorescent nanoswitch based on reversible disulfide and its application in butyrylcholinesterase activity assay. Anal Chem 90(3):1643–1651
6. Nechaeva N, Prokopkina T, Makhaeva G, Rudakova E, Boltneva N, Dishovsky C, Eremenko A, Kurochkin I (2018) Quantitative butyrylcholinesterase activity detection by surface-enhanced Raman spectroscopy. Sens Actuators, B 259:75–82
7. Yang Y, Liu H, Chen Z, Wu T, Jiang Z, Tong L, Tang B (2019) A simple 3D-printed enzyme reactor paper spray mass spectrometry platform for detecting BuChE activity in human serum. Anal Chem 91(20):12874–12881
8. Miao Y, He N, Zhu J-J (2010) History and new developments of assays for cholinesterase activity and inhibition. Chem Rev 110(9):5216–5234
9. Marton CH, Haldeman GS, Jensen KF (2011) Portable thermoelectric power generator based on a microfabricated silicon combustor with low resistance to flow. Ind Eng Chem Res 50(14):8468–8475
10. Arata HF, Rondelez Y, Noji H, Fujita H (2005) Temperature alternation by an on-chip Microheater to reveal enzymatic activity of β-galactosidase at high temperatures. Anal Chem 77(15):4810–4814
11. Yue Y, Li F, Li Y, Wang Y, Guo X, Cheng Z, Li N, Ma X, Nie G, Zhao X (2021) Biomimetic nanoparticles carrying a repolarization agent of tumor-associated macrophages for remodeling of the inflammatory microenvironment following photothermal therapy. ACS Nano. https://doi.org/10.1021/acsnano.1c05618
12. Zhang J, Xing H, Lu Y (2018) Translating molecular detections into a simple temperature test using a target-responsive smart thermometer. Chem Sci 9(16):3906–3910
13. Xue X, Luo M, Rao H, Xue Z, Wang B, Liu X, Lu X (2020) Enhanced thermometric sensor for arsenate analysis based on dual temperature readout signaling strategy. Anal Chem 92(6):4672–4680
14. Fu G, Sanjay ST, Dou M, Li X (2016) Nanoparticle-mediated photothermal effect enables a new method for quantitative biochemical analysis using a thermometer. Nanoscale 8(10):5422–5427
15. Guo L, Zhang Y-J, Yu Y-L, Wang J-H (2020) In situ generation of prussian blue by MIL-53 (Fe) for point-of-care testing of butyrylcholinesterase activity using a portable high-throughput photothermal device. Anal Chem 92(21):14806–14813
16. Ma Z, Cao L, Xing Y, Feng A, Zhang P, Li W, Nie H, Shi Y-e, Wang Z (2021) Sensitive detection of butyrylcholinesterase activity based on a separation-free photothermal assay. Microchem. J. 166:106220
17. Yan X, Song Y, Zhu C, Li H, Du D, Su X, Lin Y (2018) MnO_2 nanosheet-carbon dots sensing platform for sensitive detection of organophosphorus pesticides. Anal Chem 90(4):2618–2624
18. Zeng M, Chen M, Huang D, Lei S, Zhang X, Wang L, Cheng Z (2021) Engineered two-dimensional nanomaterials: an emerging paradigm for water purification and monitoring. Mater Horiz 8(3):758–802
19. Tong J, Xue Y, Wang J, Wang M, Chen W, Tian Q, Yu F (2020) Cu/Cu2O nanoparticle–decorated MoO2 nanoflowers as a highly efficient electrocatalyst for hydrogen evolution reaction. Energy Technol 8(7):1901392
20. Ermini ML, Voliani V (2021) Antimicrobial nano-agents: the copper age. ACS Nano 15(4):6008–6029
21. Zhang H, Zhang Z, Li N, Yan W, Zhu Z (2017) Cu_2O@C core/shell nanoparticle as an electrocatalyst for oxygen evolution reaction. J Catal 352:239–245
22. Gupta D, Meher SR, Illyaskutty N, Alex ZC (2018) Facile synthesis of Cu_2O and CuO nanoparticles and study of their structural, optical and electronic properties. J Alloys Compd 743:737–745
23. Periasamy AP, Wu W-P, Lin G-L, Shih Z-Y, Yang Z, Chang H-T (2014) Synthesis of Cu_9S_8/carbon nanotube nanocomposites with high electrocatalytic activity for the oxygen reduction reaction. J Mater Chem A 2(30):11899–11904

24. Feng L, Wu S, Wu Y (2021) Intracellular bottom-up synthesis of ultrasmall CuS nanodots in cancer cells for simultaneous photothermal therapy and CO_{X-2} inactivation. Adv Funct Mater 31(27):2101297
25. Yang N, Guo H, Cao C, Wang X, Song X, Wang W, Yang D, Xi L, Mou X, Dong X (2021) Infection microenvironment-activated nanoparticles for NIR-II photoacoustic imaging-guided photothermal/chemodynamic synergistic anti-infective therapy. Biomaterials 275:120918
26. Shi Y-e, Zhuang X, Cao L, Gou S, Xiong Y, Lai W-F, Wang Z, Rogach AL (2019) Copper-Nanocluster-Based Transparent Ultraviolet-Shielding Polymer Films. ChemNanoMat 5(1):110–115
27. Cheng Y, Lin Y, Xu J, He J, Wang T, Yu G, Shao D, Wang W-H, Lu F, Li L, Du X, Wang W, Liu H, Zheng R (2016) Surface plasmon resonance enhanced visible-light-driven photocatalytic activity in Cu nanoparticles covered Cu_2O microspheres for degrading organic pollutants. Appl Surf Sci 366:120–128
28. Schatz M, Becker M, Thaler F, Hampel F, Schindler S, Jacobson RR, Tyeklár Z, Murthy NN, Ghosh P, Chen Q, Zubieta J, Karlin KD (2001) Copper(I) complexes, copper(I)/O_2 reactivity, and copper(II) complex adducts, with a series of tetradentate tripyridylalkylamine tripodal ligands. Inorg Chem 40(10):2312–2322
29. Konopińska KK, Schmidt NJ, Hunt AP, Lehnert N, Wu J, Xi C, Meyerhoff ME (2018) Comparison of copper(II)–ligand complexes as mediators for preparing electrochemically modulated nitric oxide-releasing catheters. ACS Appl Mater Interfaces 10(30):25047–25055
30. Wang Z, Zhang C, Wang H, Xiong Y, Yang X, Shi Y-e, Rogach AL (2020) Two-step oxidation synthesis of sulfur with a red aggregation-induced emission. Angew Chem Int Ed 59(25):9997–10002
31. Fantauzzi M, Elsener B, Atzei D, Rigoldi A, Rossi A (2015) Exploiting XPS for the identification of sulfides and polysulfides. RSC Adv 5(93):75953–75963
32. Li W, Rong Y, Wang J, Li T, Wang Z (2020) MnO_2 switch-bridged DNA walker for ultrasensitive sensing of cholinesterase activity and organophosphorus pesticides. Biosens. Bioelectron. 169:112605